Hidden covalent insulator and spin excitations in $SrRu_2O_6$

Diana Csontosová,[1,2] Jiří Chaloupka,[1] Hiroshi Shinaoka,[3] Atsushi Hariki,[4] and Jan Kuneš[1,2]

[1]*Department of Condensed Matter Physics, Faculty of Science, Masaryk University, Kotlářská 2, 611 37 Brno, Czechia*

[2]*Institute for Solid State Physics, TU Wien, 1040 Vienna, Austria*

[3]*Department of Physics, Saitama University, Saitama 338-8570, Japan*

[4]*Department of Physics and Electronics, Graduate School of Engineering, Osaka Metropolitan University, 1-1 Gakuen-cho, Nakaku, Sakai, Osaka 599-8531, Japan*

(Received 2 June 2023; accepted 23 October 2023; published 17 November 2023)

The density functional plus dynamical mean-field theory is used to study the spin excitation spectra of $SrRu_2O_6$. A good quantitative agreement with experimental spin excitation spectra is found. Depending on the size of the Hund's coupling J_H, the system chooses either the Mott insulator or covalent insulator state when magnetic ordering is not allowed. We find that the nature of the paramagnetic state has a negligible influence on the charge and spin excitation spectra. We find that antiferromagnetic correlations hide the covalent insulator state for realistic choices of the interaction parameters.

DOI: 10.1103/PhysRevB.108.195137

I. INTRODUCTION

The competition between kinetic and interaction energy is the cornerstone of correlated electrons physics. In the paradigmatic bandwidth control scenario of the Hubbard model at half filling, increasing the interaction-to-bandwidth ratio suppresses the charge fluctuations and eventually drives the system to a Mott insulator (MI) state [1]. Real materials provide variations on this theme [2,3], as well as alternative mechanisms of the correlation-driven metal-insulator transition (MIT) such as site-selective Mott transition [4], spin-state crossover [5,6], Kondo insulator [7], or gapping of the ligand bands [8], to name a few. Often the paramagnetic (PM) MIT is hidden by a magnetic long-range order, which raises the question of how much about the nature of the PM phase can be learned from the properties of the ordered phase. The studies of the single-band Hubbard model [9,10] found rather subtle differences in the antiferromagnetic (AFM) phases on the two sides of the Mott transition, which can be difficult or even impossible to identify in a multiorbital setting of real materials.

A weakly correlated state does not have to be metallic in order to exhibit charge fluctuations. A covalent insulator (CI) [11], with a gap between the bonding and antibonding states, does as well. Mazin *et al.* [12] pointed out a special hopping pattern of t_{2g} electrons in layered transition-metal oxides with a honeycomb lattice and edge-sharing octahedra such as Na_2IrO_3, α-$RuCl_3$, Li_2RuO_3, or $SrRu_2O_6$. Considering only the dominant hopping paths between the nearest-neighbor metal ions, the t_{2g} electrons are trapped on the hexagonal structural units, which gives rise to molecular orbitals clearly visible in the calculated noninteracting electronic spectra. At half filling, the Fermi level falls into the band gap between the molecular peaks [13], which stabilizes the CI state. On the other hand, the tendency to form a high-spin MI is also maximal at half filling [14], which leads to a competition without an *a priori* winner. This scenario is realized in $SrRu_2O_6$ with nominally t_{2g}^3 configuration. It is an AFM insulator with high Néel temperature T_N of 563 K [16] and does not exhibit the Curie-Weiss susceptibility in the PM phase. Instead, the susceptibility increases up to the highest reported temperature of about 730 K [17]. The classification of $SrRu_2O_6$ based on numerical studies has been controversial. Streltsov *at al.* [13] performed density functional plus dynamical mean-field theory (DFT+DMFT) calculations for Hund's coupling, $J_H = 0.3$ eV. Pointing out the discrepancy between the theoretical ionic moment of $3\,\mu_B$, a value essentially reproduced by their DFT+DMFT, and the observed ordered moment of $1.4\,\mu_B$, they argued that the electronic structure of $SrRu_2O_6$ is dominated by molecular orbitals. Hariki *et al.* [18], using a similar DFT+DMFT approach, found a crossover between CI and MI in the PM phase for J_H between 0.16 and 0.19 eV, depending on temperature. They also found that in the AFM phase, the size of the ordered moment is essentially the same on both sides of the CI/MI crossover and agrees well with the experimental as well as the DFT value, when the overlaps of Wannier orbitals are properly accounted for. The uncertainty in the value of the Hund's exchange J_H thus left the question of the electronic structure of $SrRu_2O_6$ open.

Using resonant inelastic x-ray scattering (RIXS) to map out the magnon dispersion, Suzuki *et al.* [19] concluded that $SrRu_2O_6$ is a Mott insulator because the magnon spectrum can be well described by the $S = 3/2$ Heisenberg model with parameters obtained by strong-coupling expansion with first-principles hopping parameters. They pointed out the difference between a large paramagnetic Néel temperature Θ, proportional to the interatomic exchange J and reflected in the magnon bandwidth, and the smaller ordering temperature T_N, determined by the spin gap. They argued that the observed absence of Curie-Weiss behavior above T_N is consistent with the behavior of the two-dimensional (2D) Heisenberg model, for which it is expected first for $T > \Theta$.

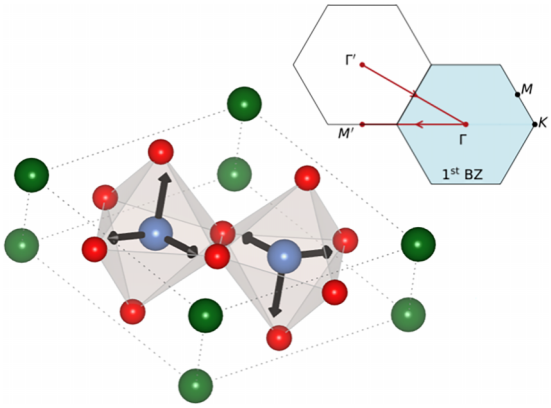

FIG. 1. The unit cell of $SrRu_2O_6$: Ru (blue), O (red), and Sr (green) atoms, visualized using VESTA3 [15]. The arrows mark the local orbital coordinates. Path in the reciprocal space used for plotting magnon dispersions.

We compute the spin excitation spectra [20,21] using DFT+DMFT [22]. We pursue two objectives: (i) apply the DMFT approach to dynamical susceptibilities based on the Bethe-Salpeter equation (BSE) [23,24] to an ordered state of a real material and assess its quantitative accuracy, and (ii) analyze the connection between the character of the PM phase, MI vs CI, and the properties of the AFM phase. The DMFT BSE approach has been successfully applied to antiferromagnetic magnons in up to the three-orbital model [24]. Here we focus on a quantitative comparison with the experiment, the role of spin-orbit coupling (SOC), the relationship between single-ion anisotropy and the spin gap, and other spin excitations beyond magnon. In order to address (ii), we vary J_H across the CI-MI crossover.

II. COMPUTATIONAL METHOD

We study the "t_{2g}-only" model of Ref. [18] with Slater-Kanamori interaction obtained by Wannierization [25,26] from density functional calculation [27]. Unlike in Ref. [18], we use the basis of xy, yz, and xz Wannier orbitals in the coordinates shown in Fig. 1; see the Supplemental Material (SM) [28] and references [29–35] therein. In order to reduce the computational effort, the calculations were done for C-type (two atoms) rather than the experimental G-type (four atoms) structure. This approach is justified by the minuscule interlayer coupling [17].

Several Ru compounds with honeycomb structure exhibit Ru-Ru dimerization upon cooling, i.e., Li_2RuO_3 [36], or under pressure, i.e., $RuCl_3$ [37] or $Ag_3LiRu_2O_6$ [38], which has been associated with a delicate balance between covalent bonding and spin-orbit entanglement [38]. Such behavior was observed neither in $SrRu_2O_6$ [17] nor in isoelectronic $BaRu_2O_6$ [39]. We speculate that this is related to the Ru d^3 configuration, which favors a high-spin moment over spin-orbit entanglement (relative to other filling) and corresponds to one electron per each Ru-Ru bond. Therefore, we perform our calculations for a fixed experimental structure.

Throughout this study, we keep the interaction parameter $U = 2.7$ eV fixed and vary $J_H = 0.16$–0.22 eV as well as temperature. In the PM calculation, we enforce the spin symmetry of the self-energy in each DMFT iteration.

The DMFT [40] calculations were performed with a multiorbital implementation [41] of the continuous-time hybridization expansion Monte Carlo method [42] based on ALPS core libraries [43]. Some of the DMFT calculations were benchmarked against results obtained with DCORE [44]. The BSE with local particle-hole irreducible vertex [45] was solved for the lowest 10 bosonic Matsubara frequencies in the Legendre representation [46]. The desired dynamical susceptibilities $\langle O_{-\mathbf{q}} O_{\mathbf{q}} \rangle_\omega$ were obtained by sandwiching the general two-particle susceptibility with the corresponding vertices followed by analytic continuation [47,48]; see the SM [28] for details. The reciprocal space operators are related to the local observable by the Fourier transform,

$$O_{\mathbf{q}} = \sum_{\mathbf{R},s} e^{-i\mathbf{q}\cdot(\mathbf{R}+\mathbf{r}_s)} O_{\mathbf{R}s}, \quad \mathbf{r}_s = \begin{cases} (\frac{2}{3}, \frac{1}{3}, 0)\ s = \mathrm{A} \\ (\frac{1}{3}, \frac{2}{3}, 0)\ s = \mathrm{B}, \end{cases} \tag{1}$$

where the index s refers to the two Ru sites in the unit cell. In the following, we study the transverse spin susceptibility with $O \equiv S^x$, and $S = 3/2 \to 1/2$ excitations, for which we choose a representative operator $O \equiv X$ below, generating $\Delta S^z = \pm 1$ transitions between the $S = 3/2$ and $S = 1/2$ manifolds,

$$S^x_{\mathbf{R}s} = \sum_{\alpha=1}^{3} \mathrm{d}^\dagger_{\mathbf{R}s\alpha\uparrow} \mathrm{d}_{\mathbf{R}s\alpha\downarrow} + \mathrm{H.c.}, \tag{2}$$

$$X_{\mathbf{R}s} = \left(\mathrm{d}^\dagger_{\mathbf{R}s1\uparrow} \mathrm{d}_{\mathbf{R}s1\downarrow} - \mathrm{d}^\dagger_{\mathbf{R}s2\uparrow} \mathrm{d}_{\mathbf{R}s2\downarrow}\right) + \mathrm{H.c.} \tag{3}$$

The operator X is chosen to be representative of a set of closely spaced transitions; see the SM [28].

III. RESULTS AND DISCUSSION

A. Magnon dispersion

The DMFT calculations lead to AFM with out-of-plane orientation of the local moment for temperatures below 1500 K. Since the magnetism of $SrRu_2O_6$ is essentially 2D [17,19], this overestimation by DMFT is expected. The DMFT does not obey the Mermin-Wagner theorem and the calculated ordering temperature represents Θ rather than T_N. This does not mean that the DMFT AFM solution should not be able to capture the ordered state of the real material. Figure 2 shows a comparison of the dynamical susceptibilities $\langle X_{-\mathbf{q}} X_{\mathbf{q}} \rangle_\omega$ and $\langle S^x_{-\mathbf{q}} S^x_{\mathbf{q}} \rangle_\omega$ calculated in the AFM phase at 464 K to the experimental RIXS data [19]. The magnetic moments at this temperature are essentially saturated [18,28] and thus no significant change in the computed spectra is expected upon further cooling. Rather than computing the full RIXS spectra, the calculation of which would require evaluation of transition amplitudes [49,50] with the possibility of multiparticle excitations [51,52] and is not possible with the present methods, we compare the dispersions of specific spectral features. We find a very good match of the magnon dispersion including the bandwidth, the spin gap, and the distribution of spectral weight. The magnon bandwidth of 183 meV corresponds to the effective nearest-neighbor exchange $JS = 61$ meV between $S = 3/2$ local moments.

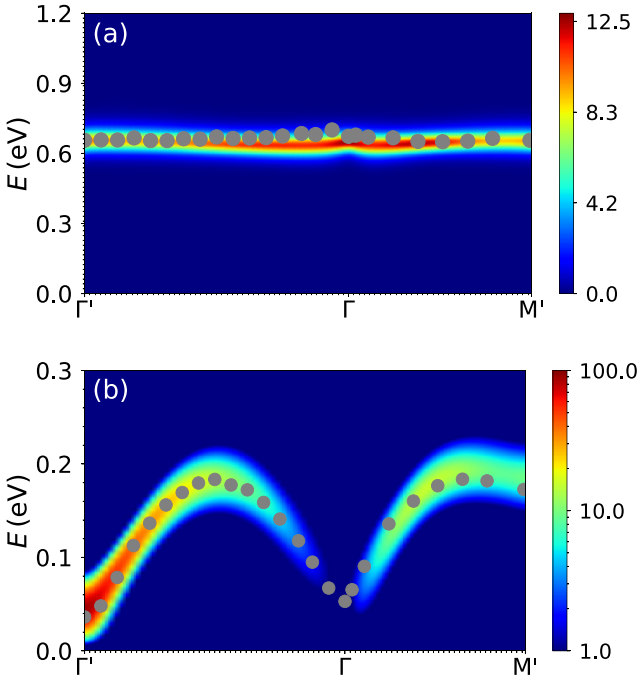

FIG. 2. Imaginary part of the dynamical susceptibility along the Γ' - Γ - M path shown in Fig. 1 for $J_H = 0.16$ eV at $T = 464$ K. Gray dots denote the maxima of the corresponding RIXS features [19]. (a) Linear color scale: $\langle X_{-\mathbf{q}} X_{\mathbf{q}} \rangle_\omega$ representing the $S = 3/2 \rightarrow 1/2$ transitions. (b) Logarithmic color scale: $\langle S^x_{-\mathbf{q}} S^x_{\mathbf{q}} \rangle_\omega$ corresponding to the magnon.

A straightforward strong-coupling calculation with the same parameter setup yields a remarkably similar value $JS \approx 66$ meV [28], essentially unaffected by SOC. However, by inspecting the exact solution of our Hubbard model on a single bond [28], we found the spin $S = 3/2$ picture to be significantly disturbed by a large involvement of higher multiplet states at energies $\gtrsim 3J_H$ [28]. In such situation, the DMFT approach covering the entire spectrum of multiplet states is highly advantageous.

The spin gap of approximately 45 meV is related to the single-ion anisotropy (SIA), $\Delta_{\mathrm{SIA}} = E_{\pm 1/2} - E_{\pm 3/2} = 6.6$ meV, defined as the difference between the atomic states belonging to the $S = 3/2$ multiplet [53]. The strong-coupling evaluation of SIA suggests that the above ionic value is actually strongly renormalized by exchange processes [28]. Within the linear spin-wave theory of the Heisenberg antiferromagnet, the large gap is easily explained even for small SIA, as it is given by $S\sqrt{6J\Delta_{\mathrm{SIA}}}$ [19]. Nevertheless, it is not self-evident that the present numerical approach must capture it accurately.

We have also carefully checked the out-of-plane orientation of the ordered moments (see SM [28]) and verified its origin in SOC by performing calculations with a SU(2)-symmetric Hamiltonian without SOC. As expected, we find two gapless linear Goldstone modes with divergent spectral weights in this case; see Fig. 3.

The experimental RIXS spectra [19] exhibit a prominent low-energy feature associated with $S = 3/2 \rightarrow 1/2$ transitions. Our calculations (Fig. 2) reproduce the position of this feature fairly well.

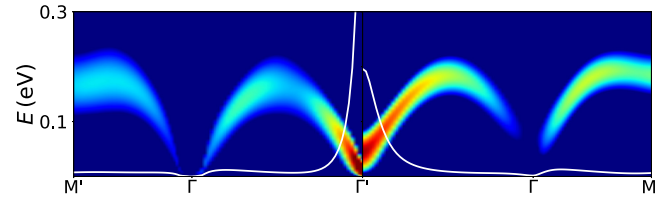

FIG. 3. Effect of the spin-orbit coupling (SOC) on the magnon spectra: with SOC (right panel) and without SOC (left panel). Color scale is the same as in Fig. 2(b). The white line is a spectral weight computed as $\Omega_{\mathbf{q}} = -\frac{1}{\pi}\int_0^{0.3} \mathrm{d}\omega\, \mathrm{Im}\langle S^x_{-\mathbf{q}} S^x_{\mathbf{q}} \rangle_\omega$. The results were obtained for $J_H = 0.16$ eV and $T = 464$ K.

B. Mott vs covalent insulator

In calculations performed in the PM state, the authors of Ref. [18] observed a crossover between the low-temperature CI and high-temperature MI at a scale $T^\star$, which strongly depends on J_H. For $J_H = 0.16$ eV, the scale $T^\star$ lies in the 600–800 K range, while for $J_H \gtrsim 0.19$ eV, only MI was observed. $SrRu_2O_6$ exists in the PM phase below 800 K; however, since DMFT exaggerates its ordering temperature [54]. we enforce the PM solution by constraint in order to study it at lower temperatures.

The different temperature scales discussed below are summarized in the inset of Fig. 4. The paramagnetic Néel temperature Θ, which we identify with the DMFT ordering temperature, is estimated from the present study, the bottom panel of Fig. 4, and Ref. [18]. The CI/MI crossover temperature $T^\star$ is estimated from Ref. [18] and the uniform susceptibility from $J_H = 0.16$ eV of this study. Finally, T_N is the experimental ordering temperature, the weak J_H dependence of which may be deduced from the behavior of the spin gap as a function of J_H.

Next, we discuss the properties of the constrained PM solutions. At high temperatures ($T > T^\star$), CI and MI behave similarly. The imaginary part of the self-energy, shown in Fig. 5, exhibits a broad peak at the chemical potential, which gives rise to a gap containing some incoherent spectral weight. At low temperatures ($T < T^\star$), CI and MI are distinguished by several characteristics. The self-energy of CI has a Fermi liquid character with vanishing imaginary part at the chemical potential. The peak in MI self-energy becomes sharper and its background vanishes in the low-energy region, which defines the Mott gap. This gives rise to the distinct band structures shown in Fig. 6. For the evolution of the self-energy on the imaginary axis, see the SM [28]. The CI and MI respond differently to a magnetic field. The magnetic susceptibility $\chi(T)$ of MI (Fig. 4) exhibits the usual Curie-Weiss decrease with increasing temperature. The high-temperature susceptibility of CI follows the same trend. However, once the Fermi liquid behavior sets in below $T^\star$ [55], the susceptibility starts to drop, which gives rise to a broad maximum. A positive slope of the experimental $\chi(T)$ above the transition temperature was pointed out by the authors of Ref. [17]. The CI and MI states are also distinguished by local charge fluctuations

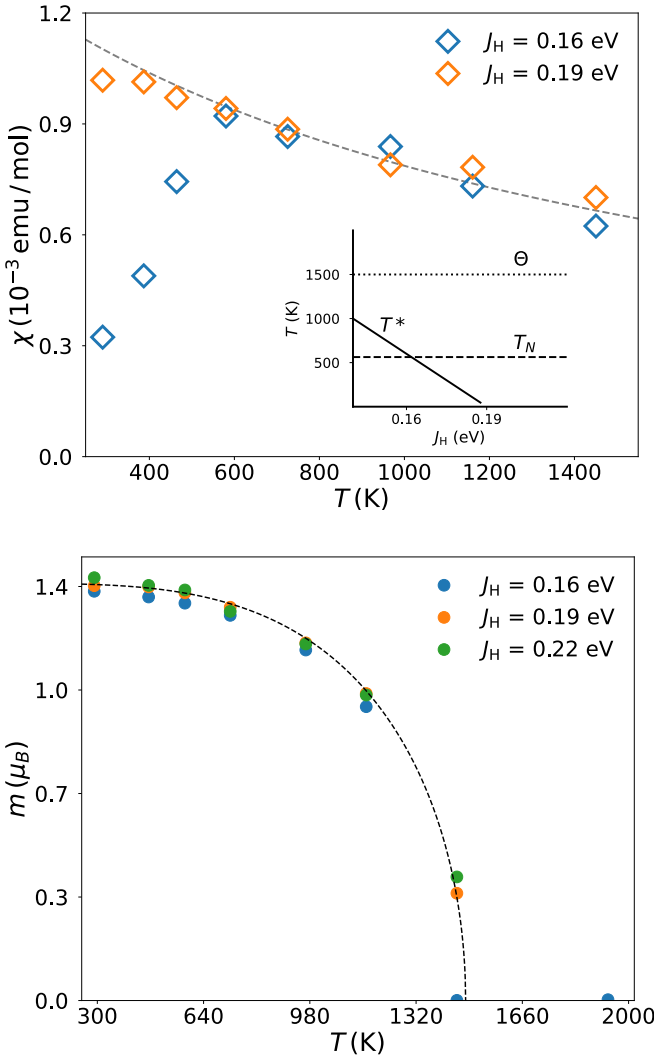

FIG. 4. Top panel: Uniform susceptibility for $J_H = 0.16$ eV and $J_H = 0.19$ eV in the PM state. The dashed line shows the Curie-Weiss susceptibility $\chi \propto (T + \Theta)^{-1}$ with $\Theta = 1480$ K. Magnitude of the calculated $\chi(T)$ is about 30% smaller than the experimental one [17]. Inset: A cartoon picture of different temperature scales in $SrRu_2O_6$. Bottom panel: Ordered moment, scaled by a factor of 0.52 to account for the overlaps of the Wannier orbitals [18], as a function of temperature for the studied values of J_H.

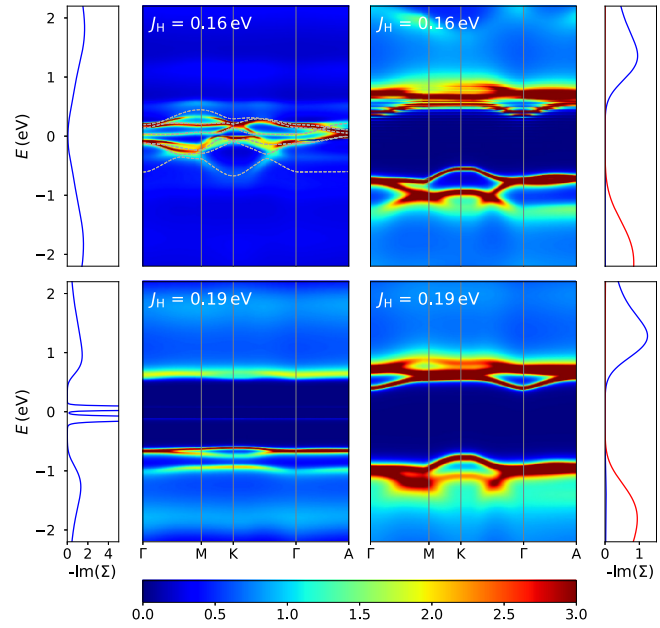

FIG. 6. Spectral functions and corresponding imaginary parts of self-energies on the real axis in the constrained PM solution (left half) and AFM solution (right half). The calculations were performed for $T = 290$ K. Red and blue colors in the figures with AFM self-energies distinguish between the spin-up and spin-down components. The gray lines in the spectral function with $J_H = 0.16$ eV show the DFT band structure squeezed by factor 2.2.

on the Ru site [18]. This is reminiscent of the site-selective Mott transition [4], where both CI- and MI-like sites are found within the same compound. Numerical simulations of core-level spectroscopies such as x-ray absorption or RIXS [56] revealed distinct dependencies on the incoming photon frequency. A similar spectroscopic signature may be expected for the CI and MI states.

How is the different character of the PM phase reflected in the AFM phase? Upon magnetic ordering, the self-energy is dominated by the spin-dependent Hartree shift, and the electronic spectra for large and small J_H in Fig. 6 resemble one another. In Fig. 7, we compare the magnon spectra obtained at 464 K for J_H values on both sides of the CI/MI crossover. A difference is hardly noticeable. There is a discernible trend of decreasing spin gap with J_H, which follows

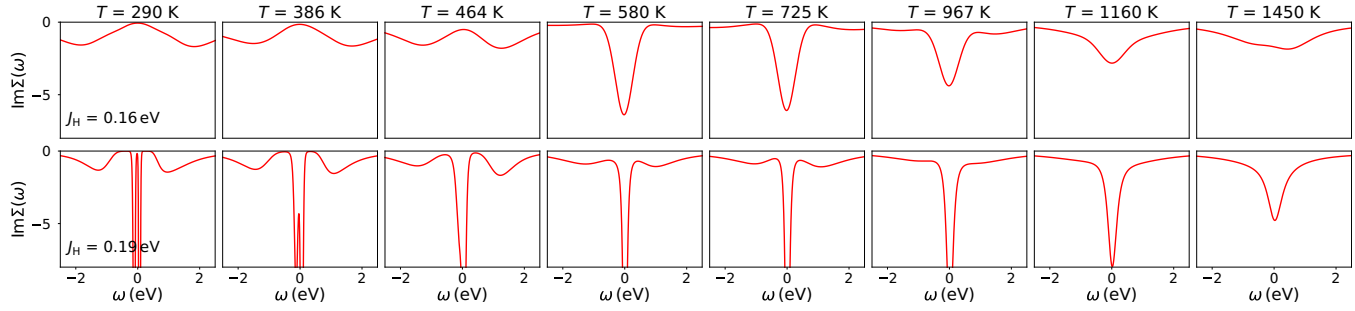

FIG. 5. Imaginary part of self-energy $\mathrm{Im}\Sigma_{ii}(\omega)$ (diagonal element) on the real frequency axis for $J_H = 0.16$ eV (top row) and $J_H = 0.19$ eV (bottom row) at various temperatures T. The crossover temperature $T^\star$ for $J_H = 0.16$ eV lies between 464 and 580 K.

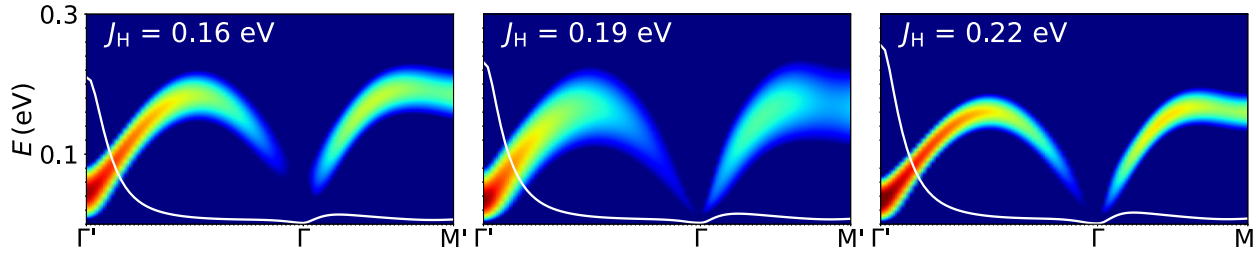

FIG. 7. Comparison of magnon spectra in covalent insulator ($J_H = 0.16$ eV) and Mott insulator ($J_H = 0.19$ eV and $J_H = 0.22$ eV) phases. The calculations were performed for $T = 464$ K. The spin gaps for $J_H = \{0.16, 0.19, 0.22\}$ eV are $\Delta_m = \{45, 36, 35\}$ meV, respectively. The white line is a spectral weight $\Omega_{\mathbf{q}}$. [The color scale is the same as in Fig. 2(b).]

from the behavior of the single-ion anisotropy. Overall, the parameters extracted using strong-coupling theory describe the magnons equally well on the CI and MI sides in the parameter space.

Can the behavior of the CI susceptibility explain the experimentally observed behavior of $\chi(T)$ in the PM phase? Is it plausible that an improved theory, which pushes the calculated T_N to its experimental value below $T^\star$, uncovers the CI susceptibility? We argue that it is not. The problem of the DMFT description is not quantitative overestimation of T_N because of inaccurate treatment of the 3D aspect (interlayer coupling) of the material. In fact, the estimated interlayer coupling [17] was shown to be, by far, too small to account for the observed T_N [19]. The problem is a conceptual inefficacy to distinguish between the paramagnetic Néel temperature Θ and the ordering temperature T_N. In fact, the Θ given by DFT+DMFT, i.e., the onset of strong AFM correlations, is likely correct as suggested by the correct magnon bandwidth obtained in the calculation. DMFT does not exaggerate the onset temperature of the AFM correlations, but describes them as static (AFM order), while in the 2D reality, they remain dynamical down to much lower temperature T_N determined by a spin gap. Although the spin gap itself is well captured, its effect on T_N is completely missing in the theory. The CI physics can be realized if the crossover temperature $T^\star$ is above the onset of AFM correlations Θ. In the present case for smaller J_H, we get $T_N < T^\star < \Theta$ and thus the increase of $\chi(T)$ above T_N represents the physics of the 2D Heisenberg magnet rather than that of CI.

We would like to point out the analogy of the present physics with the Kondo lattice model [57]. In both cases a local moment disappears below a certain temperature, i.e., $T^\star$ in CI or Kondo temperature in the case of the Kondo lattice, if not correlated to other moments on the lattice. In both cases, intersite correlations between the local moments can preclude their disappearance if they are sufficiently strong, which we conjecture to mean $T^\star < \Theta$ in the present case. These are examples of a situation when intersite interaction between the local excited states (carrying the local moments) eliminates the (nonmagnetic) local ground states from the set of global low-energy states.

IV. CONCLUSIONS

We have calculated the spin excitation spectra of $SrRu_2O_6$ using the DFT+DMFT approach and found a quantitative match with the experimental observations [19], notably for the spin gap due to the spin-orbit coupling. The paramagnetic state of $SrRu_2O_6$, depending on the strength of the Hund's coupling J_H, exhibits either covalent insulator or Mott insulator characteristics below $T^\star \approx 580$ K. Once in the AFM ordered state, the magnon and electron excitation spectra are essentially the same for J_H on both sides of the covalent-insulator/Mott-insulator crossover. Our calculations for realistic J_H on both sides of the CI/MI crossover lead to the conclusion that $T^\star$ is substantially below the temperature Θ at which the AFM correlations set in and therefore the covalent insulator state remains always "hidden."

ACKNOWLEDGMENTS

The authors thank H. Suzuki for providing the experimental data of Fig. 2, A. Kauch for critical reading of the manuscript, and K.-H. Ahn for valued discussions in the early stage of this work. This work has received funding from QUAST-FOR5249 Project No. I 5868-N (D.C., J.K.) of the Austrian Science Fund (FWF), Czech Science Foundation (GAČR) Project No. GA22-28797S (D.C., J.C.), JSPS KAKENHI Grants No. 21K13884, No. 23K03324 (A.H.), No. 21H01003, No. 23H03816, and No. 23H03817 (H.S., A.H.), Austrian Federal Ministry of Science, Research and Economy through the Vienna Scientific Cluster (VSC) Research Center, and by the Ministry of Education, Youth and Sports of the Czech Republic through the e-INFRA CZ (ID:90254). H.S. was supported by JSPS KAKENHI Grant No. 21H01041. H.S. thanks the Supercomputer Center, the Institute for Solid State Physics, and the University of Tokyo for the use of their facilities.

[1] W. F. Brinkman and T. M. Rice, Application of Gutzwiller's variational method to the metal-insulator transition, Phys. Rev. B **2**, 4302 (1970).

[2] E. Pavarini, S. Biermann, A. Poteryaev, A. I. Lichtenstein, A. Georges, and O. K. Andersen, Mott transition and suppression of orbital fluctuations in orthorhombic $3d^1$ perovskites, Phys. Rev. Lett. **92**, 176403 (2004).

[3] B. J. Kim, H. Jin, S. J. Moon, J.-Y. Kim, B.-G. Park, C. S. Leem, J. Yu, T. W. Noh, C. Kim, S.-J. Oh, J.-H. Park, V. Durairaj, G. Cao, and E. Rotenberg, Novel $J_{\text{eff}} = 1/2$ Mott state induced by

relativistic spin-orbit coupling in Sr_2IrO_4, Phys. Rev. Lett. **101**, 076402 (2008).

[4] H. Park, A. J. Millis, and C. A. Marianetti, Site-selective Mott transition in rare-earth-element nickelates, Phys. Rev. Lett. **109**, 156402 (2012).

[5] J. R. Patterson, C. M. Aracne, D. D. Jackson, V. Malba, S. T. Weir, P. A. Baker, and Y. K. Vohra, Pressure-induced metallization of the Mott insulator MnO, Phys. Rev. B **69**, 220101(R) (2004).

[6] J. Kuneš, A. V. Lukoyanov, V. I. Anisimov, R. T. Scalettar, and W. E. Pickett, Collapse of magnetic moment drives the Mott transition in MnO, Nat. Mater. **7**, 198 (2008).

[7] Z. Fisk, J. L. Sarrao, S. L. Cooper, P. G. Nyhus, G. S. Boebinger, A. Passner, and P. C. Canfield, Kondo insulators, Phys. B: Condens. Matter **223**, 409 (1996).

[8] J. Kuneš, L. Baldassarre, B. Schächner, K. Rabia, C. A. Kuntscher, D. M. Korotin, V. I. Anisimov, J. A. McLeod, E. Z. Kurmaev, and A. Moewes, Metal-insulator transition in $NiS_{2-x}Se_x$, Phys. Rev. B **81**, 035122 (2010).

[9] G. Sangiovanni, A. Toschi, E. Koch, K. Held, M. Capone, C. Castellani, O. Gunnarsson, S.-K. Mo, J. W. Allen, H.-D. Kim, A. Sekiyama, A. Yamasaki, S. Suga, and P. Metcalf, Static versus dynamical mean-field theory of Mott antiferromagnets, Phys. Rev. B **73**, 205121 (2006).

[10] L. Fratino, P. Sémon, M. Charlebois, G. Sordi, and A.-M. S. Tremblay, Signatures of the Mott transition in the antiferromagnetic state of the two-dimensional Hubbard model, Phys. Rev. B **95**, 235109 (2017).

[11] C. Fu and S. Doniach, Model for a strongly correlated insulator: FeSi, Phys. Rev. B **51**, 17439 (1995); J. Kuneš and V. I. Anisimov, Temperature-dependent correlations in covalent insulators: Dynamical mean-field approximation, *ibid.* **78**, 033109 (2008); M. Sentef, J. Kuneš, P. Werner, and A. P. Kampf, Correlations in a band insulator, *ibid.* **80**, 155116 (2009).

[12] I. I. Mazin, H. O. Jeschke, K. Foyevtsova, R. Valentí, and D. I. Khomskii, Na_2IrO_3 as a molecular orbital crystal, Phys. Rev. Lett. **109**, 197201 (2012).

[13] S. Streltsov, I. I. Mazin, and K. Foyevtsova, Localized itinerant electrons and unique magnetic properties of $SrRu_2O_6$, Phys. Rev. B **92**, 134408 (2015).

[14] A. Georges, L. de Medici, and J. Mravlje, Strong correlations from Hund's coupling, Annu. Rev. Condens. Matter Phys. **4**, 137 (2013).

[15] K. Momma and F. Izumi, *VESTA3* for three-dimensional visualization of crystal, volumetric and morphology data, J. Appl. Crystallogr. **44**, 1272 (2011).

[16] C. I. Hiley, M. R. Lees, J. M. Fisher, D. Thompsett, S. Agrestini, R. I. Smith, and R. I. Walton, Ruthenium(V) oxides from low-temperature hydrothermal synthesis, Angew. Chem. Intl. Ed. **53**, 4423 (2014).

[17] C. I. Hiley, D. O. Scanlon, A. A. Sokol, S. M. Woodley, A. M. Ganose, S. Sangiao, J. M. De Teresa, P. Manuel, D. D. Khalyavin, M. Walker, M. R. Lees, and R. I. Walton, Antiferromagnetism at $T = 500 >$ K in the layered hexagonal ruthenate $SrRu_2O_6$, Phys. Rev. B **92**, 104413 (2015).

[18] A. Hariki, A. Hausoel, G. Sangiovanni, and J. Kuneš, DFT+DMFT study on soft moment magnetism and covalent bonding in $SrRu_2O_6$, Phys. Rev. B **96**, 155135 (2017).

[19] H. Suzuki, H. Gretarsson, H. Ishikawa, K. Ueda, Z. Yang, H. Liu, H. Kim, D. Kukusta, A. Yaresko, M. Minola, J. A. Sears, S. Francoual, H.-C. Wille, J. Nuss, H. Takagi, B. J. Kim, G. Khaliullin, H. Yavaş, and B. Keimer, Spin waves and spin-state transitions in a ruthenate high-temperature antiferromagnet, Nat. Mater. **18**, 563 (2019).

[20] H. Park, K. Haule, and G. Kotliar, Magnetic excitation spectra in $BaFe_2As_2$: A two-particle approach within a combination of the density functional theory and the dynamical mean-field theory method, Phys. Rev. Lett. **107**, 137007 (2011).

[21] L. Boehnke and F. Lechermann, Getting back to Na_xCoO_2: Spectral and thermoelectric properties, Phys. Stat. Solid. (a) **211**, 1267 (2014).

[22] G. Kotliar, S. Y. Savrasov, K. Haule, V. S. Oudovenko, O. Parcollet, and C. A. Marianetti, Electronic structure calculations with dynamical mean-field theory, Rev. Mod. Phys. **78**, 865 (2006).

[23] J. Kuneš, Efficient treatment of two-particle vertices in dynamical mean-field theory, Phys. Rev. B **83**, 085102 (2011).

[24] A. Niyazi, D. Geffroy, and J. Kuneš, Antiferromagnetic magnons and local anisotropy: Dynamical mean-field study, Phys. Rev. B **104**, 075152 (2021).

[25] A. A. Mostofi, J. R. Yates, G. Pizzi, Y.-S. Lee, I. Souza, D. Vanderbilt, and N. Marzari, An updated version of WANNIER90: A tool for obtaining maximally-localised Wannier functions, Comput. Phys. Commun. **185**, 2309 (2014).

[26] J. Kuneš, R. Arita, P. Wissgott, A. Toschi, H. Ikeda, and K. Held, WIEN2WANNIER: From linearized augmented plane waves to maximally localized Wannier functions, Comput. Phys. Commun. **181**, 1888 (2010).

[27] P. Blaha, K. Schwarz, G. K. H. Madsen, D. Kvasnicka, J. Luitz, R. Laskowski, F. Tran, and L. D. Marks, *WIEN2k, An Augmented Plane Wave + Local Orbitals Program for Calculating Crystal Properties* (Karlheinz Schwarz, Techn. Universität Wien, Austria, 2018); P. Blaha, K. Schwarz, F. Tran, R. Laskowski, G. K. H. Madsen, and L. D. Marks, WIEN2k An APW+lo program for calculating the properties of solids, J. Chem. Phys. **152**, 074101 (2020).

[28] See Supplemental Material at http://link.aps.org/supplemental/10.1103/PhysRevB.108.195137 for contains the computational details, definitions of two-particle correlation functions and strong-coupling analysis.

[29] A. Georges, G. Kotliar, W. Krauth, and M. Rozenberg, Dynamical mean-field theory of strongly correlated fermion systems and the limit of infinite dimensions, Rev. Mod. Phys. **68**, 13 (1996).

[30] E. Gull, A. J. Millis, A. I. Lichtenstein, A. N. Rubtsov, M. Troyer, and P. Werner, Continuous-time Monte Carlo methods for quantum impurity models, Rev. Mod. Phys. **83**, 349 (2011).

[31] P. P. Stavropoulos, X. Liu, and H.-Y. Kee, Magnetic anisotropy in spin-3/2 with heavy ligand in honeycomb Mott insulators: Application to CrI_3, Phys. Rev. Res. **3**, 013216 (2021).

[32] M. Jarrell and J. E. Gubernatis, Bayesian inference and the analytic continuation of imaginary-time quantum Monte Carlo data, Phys. Rep. **269**, 133 (1996).

[33] J. P. Perdew, K. Burke, and M. Ernzerhof, Generalized gradient approximation made simple, Phys. Rev. Lett. **77**, 3865 (1996).

[34] X. Wang, E. Gull, L. de' Medici, M. Capone, and A. J. Millis, Antiferromagnetism and the gap of a Mott insulator: Results

from analytic continuation of the self-energy, Phys. Rev. B **80**, 045101 (2009).

[35] X. Liu, D. Churchill, and H.-Y. Kee, Theoretical analysis of single-ion anisotropy in d^3 Mott insulators, Phys. Rev. B **106**, 035122 (2022).

[36] Y. Miura, Y. Yasui, M. Sato, N. Igawa, and K. Kakurai, New-type phase transition of Li_2RuO_3 with honeycomb structure, J. Phys. Soc. Jpn. **76**, 033705 (2007).

[37] G. Bastien, G. Garbarino, R. Yadav, F. J. Martinez-Casado, R. Beltrán Rodríguez, Q. Stahl, M. Kusch, S. P. Limandri, R. Ray, P. Lampen-Kelley, D. G. Mandrus, S. E. Nagler, M. Roslova, A. Isaeva, T. Doert, L. Hozoi, A. U. B. Wolter, B. Büchner, J. Geck, and J. van den Brink, Pressure-induced dimerization and valence bond crystal formation in the Kitaev-Heisenberg magnet α-$RuCl_3$, Phys. Rev. B **97**, 241108(R) (2018).

[38] T. Takayama, M. Blankenhorn, J. Bertinshaw, D. Haskel, N. A. Bogdanov, K. Kitagawa, A. N. Yaresko, A. Krajewska, S. Bette, G. McNally, A. S. Gibbs, Y. Matsumoto, D. P. Sari, I. Watanabe, G. Fabbris, W. Bi, T. I. Larkin, K. S. Rabinovich, A. V. Boris, H. Ishii *et al.*, Competing spin-orbital singlet states in the $4d^4$ honeycomb ruthenate $Ag_3LiRu_2O_6$, Phys. Rev. Res. **4**, 043079 (2022).

[39] T. Marchandier, G. Rousse, Q. Jacquet, A. M. Abakumov, F. Fauth, C. V. Colin, and J.-M. Tarascon, Magnetic and intercalation properties of $BaRu_2O_6$ and $SrRu_2O_6$, Chem. Mater. **32**, 8471 (2020).

[40] W. Metzner and D. Vollhardt, Correlated lattice fermions in $d = \infty$ dimensions, Phys. Rev. Lett. **62**, 324 (1989); A. Georges and G. Kotliar, Hubbard model in infinite dimensions, Phys. Rev. B **45**, 6479 (1992); M. Jarrell, Hubbard model in infinite dimensions: A quantum Monte Carlo study, Phys. Rev. Lett. **69**, 168 (1992).

[41] H. Shinaoka, E. Gull, and P. Werner, Continuous-time hybridization expansion quantum impurity solver for multi-orbital systems with complex hybridizations, Comput. Phys. Commun. **215**, 128 (2017).

[42] P. Werner, A. Comanac, L. de' Medici, M. Troyer, and A. J. Millis, Continuous-time solver for quantum impurity models, Phys. Rev. Lett. **97**, 076405 (2006).

[43] A. Gaenko, A. E. Antipov, G. Carcassi, T. Chen, X. Chen, Q. Dong, L. Gamper, J. Gukelberger, R. Igarashi, S. Iskakov, M. Könz, J. P. F. LeBlanc, R. Levy, P. N. Ma, J. E. Paki, H. Shinaoka, S. Todo, M. Troyer, and E. Gull, Updated core libraries of the ALPS project, Comput. Phys. Commun. **213**, 235 (2017); B. Bauer, L. D. Carr, H. G. Evertz, A. Feiguin, J. Freire, S. Fuchs, L. Gamper, J. Gukelberger, E. Gull, S. Guertler, A. Hehn, R. Igarashi, S. V. Isakov, D. Koop, P. N. Ma, P. Mates, H. Matsuo, O. Parcollet, G. Pawłowski, J. D. Picon *et al.*, The ALPS project release 2.0: Open source software for strongly correlated systems, J. Stat. Mech. Theory Expt. (2011) P05001.

[44] H. Shinaoka, J. Otsuki, M. Kawamura, N. Takemori, and K. Yoshimi, DCore: Integrated DMFT software for correlated electrons, SciPost Phys. **10**, 117 (2021).

[45] V. Zlatic and B. Horvatic, The local approximation for correlated systems on high dimensional lattices, Solid State Commun. **75**, 263 (1990).

[46] L. Boehnke, H. Hafermann, M. Ferrero, F. Lechermann, and O. Parcollet, Orthogonal polynomial representation of imaginary-time Green's functions, Phys. Rev. B **84**, 075145 (2011).

[47] D. Geffroy, J. Kaufmann, A. Hariki, P. Gunacker, A. Hausoel, and J. Kuneš, Collective modes in excitonic magnets: Dynamical mean-field study, Phys. Rev. Lett. **122**, 127601 (2019).

[48] R. Levy, J. P. F. LeBlanc, and E. Gull, Implementation of the maximum entropy method for analytic continuation, Comput. Phys. Commun. **215**, 149 (2017).

[49] A. Hariki, M. Winder, T. Uozumi, and J. Kuneš, LDA + DMFT approach to resonant inelastic x-ray scattering in correlated materials, Phys. Rev. B **101**, 115130 (2020).

[50] M. W. Haverkort, Theory of resonant inelastic x-ray scattering by collective magnetic excitations, Phys. Rev. Lett. **105**, 167404 (2010).

[51] A. Nag, H. C. Robarts, F. Wenzel, J. Li, H. Elnaggar, R.-P. Wang, A. C. Walters, M. García-Fernández, F. M. F. de Groot, M. W. Haverkort, and K.-J. Zhou, Many-body physics of single and double spin-flip excitations in NiO, Phys. Rev. Lett. **124**, 067202 (2020).

[52] J. Li, Y. Gu, Y. Takahashi, K. Higashi, T. Kim, Y. Cheng, F. Yang, J. Kuneš, J. Pelliciari, A. Hariki, and V. Bisogni, Single- and multimagnon dynamics in antiferromagnetic $\alpha-Fe_2O_3$ thin films, Phys. Rev. X **13**, 011012 (2023).

[53] The spin quantization axis is pointing out of plane.

[54] As discussed in Ref. [19], $SrRu_2O_6$ is essentially a 2D material with T_N determined by the spin gap. The dimensionality aspect is not properly captured by DMFT.

[55] Note that calculations in Ref. [18] put $T^\star$ to around 800 K.

[56] R. J. Green, M. W. Haverkort, and G. A. Sawatzky, Bond disproportionation and dynamical charge fluctuations in the perovskite rare-earth nickelates, Phys. Rev. B **94**, 195127 (2016); Y. Lu, D. Betto, K. Fürsich, H. Suzuki, H.-H. Kim, G. Cristiani, G. Logvenov, N. B. Brookes, E. Benckiser, M. W. Haverkort, G. Khaliullin, M. Le Tacon, M. Minola, and B. Keimer, Site-selective probe of magnetic excitations in rare-earth nickelates using resonant inelastic x-ray scattering, Phys. Rev. X **8**, 031014 (2018); M. Winder, A. Hariki, and J. Kuneš, X-ray spectroscopy of the rare-earth nickelate $LuNiO_3$: LDA + DMFT study, Phys. Rev. B **102**, 085155 (2020).

[57] S. Doniach, The Kondo lattice and weak antiferromagnetism, Physica B+C **91**, 231 (1977).